J Electr Eng Technol.2018; 13(?): 1921-718
http://doi.org/10.???/JEET.2018.13.2.1921

ISSN(Print) 1975-0102
ISSN(Online) 2093-7423

# Calculation of Electromagnetic Excitation Forces in Double Skewed Motors

**Xiaohua Bao†, Chong Di* and Yang Zhou****

**Abstract** – An electromagnetic excitation force is caused by the air-gap flux density, which greatly influences the noise and vibration of the motor. In many real projects, skewed slot technology is widely used to reduce the harmonic components of the air-gap flux density to reduce the noise and vibration of the motor. However, a skewed slot has several side effects such as a transverse current and axial drifting. Thus, a double skewed slot rotor is selected with the aim of eliminating these side effects. This paper presents the exact structure of the double skewed slot rotor and the mechanism whereby the electromagnetic excitation force can be reduced. A multi-slice method is adopted to model the special structure. Finite element simulation is used to verify the theory.

**Keywords**: Electromagnetic excitation force, Double skewed rotor, Multi-slice method, Finite element method



## 1. Introduction

Levels of noise and vibration have been a very important technical index of electrical machines in recent years. Electromagnetic noise and vibration are often induced by the electromagnetic excitation force resulting from the air-gap flux density [1-2]. Skewed slot technology is commonly applied to reduce the noise and vibration of the motor. Although the technology has been used in many real applications for almost one hundred years, it has nevertheless attracted many scholars' attention of late. For example, Xia et al. developed an analytical model for surface-mounted permanent magnet machines with skewed slots and verified the correctness with 3D finite element analysis [3]. Karmaker et al. developed a computational model to predict the air-gap flux density and other electromagnetic parameters [4]. In consideration of the electromagnetic force and vibration force, Hirotsuka et al. discussed the effects of the skewed slot on the electromagnetic force and vibration both theoretically and experimentally [5]. Im et al. considered the influence of the skew by coupling several disks cut by planes perpendicular to the shaft and found that the noise could be reduced by adjusting a proper skew angle of the rotor [6].

The rapid development of computer technology has enabled the simulation of the skewed slot structure by a finite element method rather than simply discussing it theoretically. Many scholars have focused on 3D finite element analysis. Kometani et al. put forward a new method using a regular coupling mesh to analyse an induction motor with skewed slots [7]. Yamada et al. proposed a simplified 3D model for a skewed rotor [8]. Yamazaki used a combination of 2D and 3D methods to consider the effects of the skewed slots [9]. The 3D model is certainly more accurate, but this model occupies too much computer memory and remains time consuming, regardless of all kinds of simplifications. Thus, the 2D model remains the mainstream model because of its computational efficiency and relative convenience. Therefore, many scholars have proposed different kinds of equivalent 2D models to substitute the complex 3D model to save computer resources [10- 13].

As mentioned above, many scholars have made contributions to skewed rotors and they have discovered many advantages of the skewed slot structure. However, they also found many unwanted side effects, such as transverse current, axial drifting, and additional eddy current losses, especially in a relatively large motor [14-15].

Our previous work had the goal of designing of an ultra-quiet induction motor, and led to the proposal of a novel skewed rotor, i.e. a double skewed rotor without a middle ring [16]. The rotor was divided into four parts along the shaft with each part oriented towards the reverse directions. However, a similar structure named herringbone tooth has already been studied, and applied in permanent magnetic motors, although it seldom appears in induction motors [17-18]. However, the different parts of the rotor are interlaced in permanent magnetic motors, such that the harmonics in different parts may be opposite and they may be reduced to a greater extent. Hence, in this paper, we propose a double skewed rotor with a middle ring. The rotor current in the induction motor is induced from the air-gap flux density and the rotor current is required to develop

† Corresponding Author: School of Electrical Engineering and Automation, Hefei University of Technology, P.R. China. (sukz@ustc.edu)
* School of Energy System, Lappeenranta University of Technology, Finland. (Chong.Di@lut.fi)
** School of Electrical Engineering and Automation, Hefei University of Technology, P.R. China. (zy284@mail.hfut.edu.cn)
Received: January 20, 2016; Accepted: November 4, 2017

a loop; thus, a middle ring is essential to connect the rotor current in different parts of the skewed rotor. The mechanism according to which the novel structure reduces the harmonics of the air-gap flux density and the electromagnetic excitation force is analysed theoretically. A simulation is carried out by modelling a modified and special multi-slice method of the double skewed rotor by adding a different stator voltage excitation and changing the rotor mechanical angle. The theoretical analysis indicates that both the double skewed rotor and the multi-slice model are correct. A finite element method is applied to construct the multi-slice model. The amplitudes of the air-gap flux density can be obtained by finite element simulation and the amplitudes of the electromagnetic excitation force can be calculated. This lays the foundation for further research on the analysis of the noise and vibration of the motor. The simulation results verify the correctness of the theory.

## 2. Analysis of Electromagnetic Excitation Force in Double Skewed Rotor Motor

Normal skewed rotors are widely used to manufacture electrical machines, especially in small- and medium-sized electrical machines to reduce noise and vibration. However, double skewed rotors have an advantage over normal rotors, particularly in improving the quality of the air-gap flux waves, reducing noise and vibration, reducing torque ripple, and so on. Fig. 1 shows the simplified structure of a double skewed rotor with two layers. Actually, the layers of can be divided into more than 2 and it can be 4, 6, 8 and so on. However, the more layers it means more difficult to manufacture. The main structure of the rotor is similar to that of normal rotors, except that the bar has been divided into two parts along the shaft, with each part being skew towards the opposite direction. Furthermore, the rotor contains an additional ring in the middle of the rotor to connect the two different skews. This ensures that there is an electrical coupling between the two different parts. In addition, all the parameters of the two skews are the same.

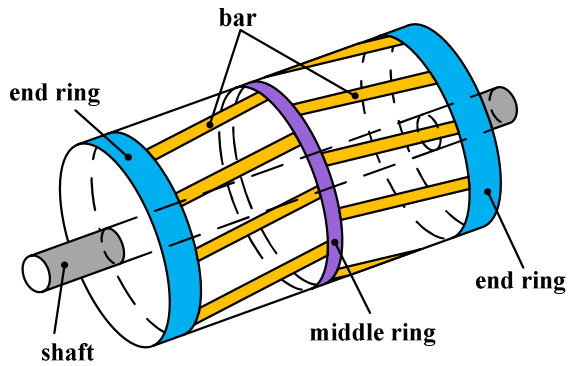


**Fig. 1.** Simplified structure of a double skewed rotor

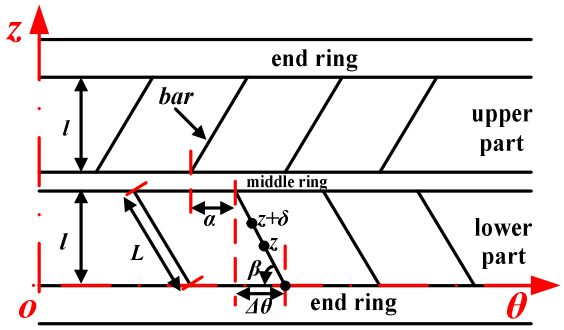


**Fig. 2.** Expanded structure of a double skewed rotor

### 2.1 Mechanism of reducing the tooth harmonics

Conventional theory shows that the skewed slots are mainly designed to reduce the harmonics of the air-gap flux density, especially the tooth harmonics. The double skewed rotor consists of two normal skews that also serve the purpose of reducing the harmonics. In this work, we use an analytical method to determine the mechanism according to which the harmonics are reduced in the novel skewed rotor. Assuming the machine is supplied with a three-phase symmetrical current source, because of the distributed winding and slotting on both the stator and rotor, the air gap gives rise to many harmonics, which have a great influence on the vibration and noise. Fig. 2 illustrates the expanded structure of a double skewed rotor.

If there are no skewed slots other than the straight slots on the stator, the harmonics produced on the lower part of the stator side area can be expressed as [19]

$$b_{1,\nu}(\theta,t) = B_\nu \cos(\nu\theta - \omega_1 t - \varphi_\nu) \tag{1}$$

where $\theta$ is the stator position from a reference point, $t$ is the time, $B_\upsilon$ is the amplitude of the harmonic, $\omega_1$ is the power supply angular frequency, $\varphi_\upsilon$ is the initial phase angle, and $\upsilon$ is the harmonic order. When the main tooth harmonics are taken into consideration, it can be expressed in the following forms

$$\nu = k\frac{Z_1}{p} \pm 1 \quad k = 0, \pm 1, \pm 2, \cdots \tag{2}$$

where $Z_1$ is the number of stator slots, and $p$ is the number of pole pairs. The acquisition of an induced current through the rotor bar, requires the induced electromotive force to be calculated first. According to Faraday's law of electromagnetic induction, and taking the straight slot into consideration, the distribution of the induced electromotive force can be expressed as

$$E(\theta,t,z) = B_\nu \cos(\nu\theta - \omega_1 t - \varphi_\nu) z v_s \tag{3}$$

where $v_s$ is the relative velocity between the rotor and the

rotated electromagnetic field, and $z$ is the axial length along the shaft in Fig. 2. It can be seen from (3) that the induced electromotive force is related to the stator position $\theta$, time $t$, and axial length $z$, and it will change with all these parameters.

When taking the skewed slot into consideration and assuming a neighbourhood $\delta$ around point $z$, the distribution of the induced electromotive force at point $z$ can be expressed as

$$E(\theta,t,z)=\int_{z}^{z+\delta} B_{\nu}\cos(\nu\theta-\omega_1 t-\varphi_{\nu}-\Delta\varphi)v_s\sin\beta dL \quad (4)$$

where $\beta$ is the mechanical angle between the skewed bar and the horizontal position in Fig. 2, $\Delta\varphi$ is the angle difference between the arbitrary point $z$ on the bar and neighbourhood point $z+\delta$, and $L$ is the length of the bar. The equation above indicates that the induced electromotive force will vary with the $z$. Taking an arbitrary point $z$ in Fig. 2 into consideration, the distribution function of the bar length can be described as

$$L(z)=\frac{z}{\sin\beta} \quad (5)$$

The angle difference at point $z$ and point $z+\delta$ can be also described with a $z$ function

$$\Delta\varphi(z)=\nu\frac{\Delta\theta z}{l}=\nu\frac{b_{sk}z}{Rl} \quad (6)$$

where $\Delta\theta$ is the skew angle in Fig. 2, $b_{sk}$ is the skew width of the bar, $l$ is the axial length of the bar and $R$ is the outer diameter of the rotor. By substituting (5) and (6) into (4), the equation can be transformed into the following forms

$$\begin{aligned}E(\theta,t,z)&=\int_{z}^{z+\delta} B_{\nu}\cos(\nu\theta-\omega_1 t-\varphi_{\nu}-\nu\frac{b_{sk}z}{Rl})v_s dz\\&=2\frac{Rlv_sB_{\nu}}{\nu b_{sk}}\cos(\nu\theta-\omega_1 t-\varphi_{\nu}-\nu\frac{b_{sk}z}{Rl}-\nu\frac{b_{sk}\delta}{2Rl})\sin\nu\frac{b_{sk}\delta}{2Rl}\end{aligned} \quad (7)$$

As $\delta\approx 0$, and assuming the angle in the neighbourhood is constant, (7) can be transformed into the following forms

$$E(\theta,t,z)=\frac{B_{\nu}\delta v_s}{\nu}\cos(\nu\theta-\omega_1 t-\varphi_{\nu}-\nu\frac{b_{sk}z}{Rl}) \quad (8)$$

The equation above indicates that the stator harmonic at point $z$ will produce induced electromotive force in the rotor bar. Assuming the resistance of a single rotor bar is $r_b$, the induced current in a single rotor bar can be expressed as

$$I(\theta,t,z)=\frac{B_{\nu}\delta v_s}{\nu r_b}\cos(\nu\theta-\omega_1 t-\varphi_{\nu}-\nu\frac{b_{sk}z}{Rl}) \quad (9)$$

The number of turns of the rotor bar is only one; thus, the magnetomotive force caused by the induced current can be expressed as follows

$$F(\theta,t,z)=NI=\frac{B_{\nu}\delta v_s}{\nu r_b}\cos(\nu\theta-\omega_1 t-\varphi_{\nu}-\nu\frac{b_{sk}z}{Rl}) \quad (10)$$

where $N$ is the number of turns of the rotor bar. According to classical theory, and assuming the air-gap permeance is $\Lambda_0$, the induced flux density can be defined as

$$b'_{1,\nu}(\theta,t,z)=F\Lambda_0=B'_{\nu}\cos(\nu\theta-\omega_1 t-\varphi_{\nu}-\nu\frac{b_{sk}z}{Rl}) \quad (11)$$

where $B'\upsilon$ is the amplitude of the induced flux density. In real projects, in order to suppress the force to the minimum, $b_{sk}$ is often selected as a stator tooth pitch of the stator. Thus,

$$\nu\frac{b_{sk}z}{Rl}=(k\frac{Z_1}{p}\pm 1)\cdot\frac{2p\pi}{Z_1}\approx 2k_1\pi \quad (12)$$

The two equations above indicate that the induced flux density have the same order, i.e. the frequency with the harmonics, which produces the induced flux density. However, the angle of the induced flux density lags about $2k_1\pi$ behind that of the origin. The interaction of the stator harmonics and the induced flux density can reduce the total harmonics. This is the mechanism according to which the skewed slots can reduce the tooth harmonics.

In consideration of the upper part of the stator side, the induced flux density caused by the stator harmonics in (1) can be expressed with almost the same equation

$$b'_{2,\nu}(\theta,t,z)=B'_{\nu}\cos(\nu\theta-\omega_1 t-\varphi_{\nu}-\nu\frac{b_{sk}z}{Rl}-\nu\alpha) \quad (13)$$

where $\alpha$ is the angle difference between the lower and upper parts and $\alpha$ is a very important parameter in the design of the double skewed slot rotor. This parameter has a direct influence on the synthesis of the electromagnetic excitation force and will be discussed next.

### 2.2 Analysis of electromagnetic excitation force

The analysis above shows how the skewed slot rotor reduced the tooth harmonics. And (11) and (13) give the exact induced flux density produced by $\upsilon^{th}$ stator harmonics. As a matter fact, there are more harmonics in the rotor sides caused by different harmonics, and they can be described as

$$\begin{cases} b'_{1,\mu}(\theta,t,z) = B'_{\mu}\cos(\mu\theta-\omega_{\mu}t-\varphi_{\mu}-\mu\dfrac{b_{sk}z}{Rl}) \\ b'_{2,\nu}(\theta,t,z) = B'_{\mu}\cos(\mu\theta-\omega_{\mu}t-\varphi_{\mu}-\mu\dfrac{b_{sk}z}{Rl}-\mu\alpha) \end{cases} \quad (14)$$

where $\omega_{\mu}$ is the frequency of the rotor harmonic, $\mu$ is the order of the rotor harmonic and it can be defined as

$$\mu = k\frac{Z_2}{p}\pm 1 \quad k=0,\pm1,\pm2,\cdots \quad (15)$$

where $Z_2$ is the number of the rotor slots. According to (1) and (14), based on Maxwell stress tensor method in [12], the electromagnetic excitation force can be calculated as the following forms

$$\begin{cases} p_{1n}(\theta,t,z) = \dfrac{2b_{1,\nu}b'_{1,\mu}}{2\mu_0} = P_{1n}\cos(n\theta-\omega_n t-\varphi_n-\mu\dfrac{b_{sk}z}{Rl}) \\ p_{2n}(\theta,t,z) = \dfrac{2b_{2,\nu}b'_{2,\mu}}{2\mu_0} = P_{2n}\cos(n\theta-\omega_n t-\varphi_n-\mu\dfrac{b_{sk}z}{Rl}-\mu\alpha) \end{cases} \quad (16)$$

where $\mu_0$ is the permeability of vacuum, $n$ is the order of the electromagnetic excitation force and $\omega_n$ is the angular frequency and $\varphi_n$ is the difference of the angle. All these parameters can be described as

$$P_{1n} = P_{2n} = \frac{B_{\nu}B'_{\mu}}{2\mu_0}, \quad n=\mu\pm\nu, \quad \omega_n = \omega_{\mu}\pm\omega_{\nu} \quad (17)$$

It can be seen from (15) that the electromagnetic excitation forces of the two different parts are almost the same expect that there is an angle between the two parts. And it is obvious that the both of the two electromagnetic excitation forces will change with $z$ position. Thus, the average electromagnetic force along $z$ axis can be determined as

$$\begin{aligned} p_{1ave}(\theta,t,z) &= \frac{1}{l}\int_{-l/2}^{l/2} p_{1n}(\theta,t,z)dz \\ &= -\frac{P_{1n}}{l}\frac{Rl}{\mu b_{sk}}\sin(n\theta-\omega_n t-\varphi_n-\mu\frac{b_{sk}z}{Rl})\Big|_{-l/2}^{l/2} \\ &= -\frac{P_{1n}R}{\mu b_{sk}}\cdot 2\cos(n\theta-\omega_n t-\varphi_n)\sin(-\mu\frac{b_{sk}}{R}) \\ &= P_{1n}\frac{\sin\mu b_{sk}/2R}{\mu b_{sk}/2R}\cos(n\theta-\omega_n t-\varphi_n) \end{aligned} \quad (18)$$

Similarly, the average electromagnetic excitation force of the upper part can be described as

$$\begin{aligned} p_{2ave}(\theta,t,z) &= \frac{1}{l}\int_{-l/2}^{l/2} p_{2n}(\theta,t,z)dz \\ &= P_{2n}\frac{\sin\mu b_{sk}/2R}{\mu b_{sk}/2R}\cos(n\theta-\omega_n t-\varphi_n-\mu\alpha) \end{aligned} \quad (19)$$

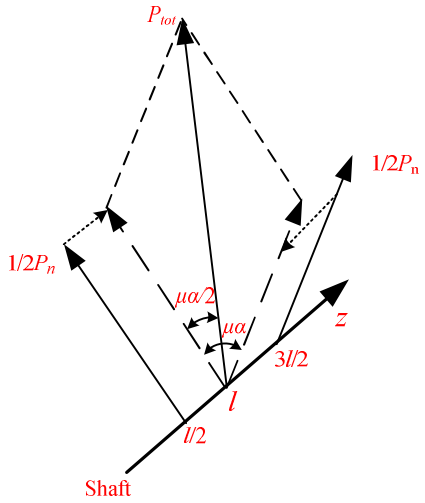


**Fig. 3.** Vector diagram of electromagnetic excitation forces

It can be seen that the average electromagnetic excitation forces in (17) and (18) are calculated in consideration of their own parts. Take the whole length into consideration, the total average electromagnetic excitation forces of each part should be divided by two, as the whole length is the twice the length of each part.

Fig. 3 shows the vector diagram of the different electromagnetic excitation forces along the shaft. It shows the electromagnetic forces in the two different skewed slot areas have the different phases. The face phase difference between the two forces in different skewed areas is $\mu\alpha$. Finally, the synthetic electromagnetic excitation force can be expressed as

$$P_{tot} = P_n\frac{\sin\mu b_{sk}/2R}{\mu b_{sk}/2R}\cos\frac{\mu\alpha}{2} \quad (20)$$

where $P_n$=$P_{1n}$=$P_{2n}$. According to the equation above, if an appropriate parameter $\alpha$ is selected, the total electromagnetic excitation force may become very small even zero. In order to make the electromagnetic excitation force as small as possible, assumption has been made as follows

$$\cos\frac{\mu\alpha}{2} = 0 \quad (21)$$

In general, $\alpha$ is selected as $t_2/2$, $t_2$ is the rotor pitch. Thus,

$$\cos\frac{\mu\alpha}{2} = \cos\frac{1}{2}(\frac{kZ_2}{p}\pm 1)\cdot\frac{p\pi}{Z_2} \approx 0 \quad (22)$$

All the analysis above indicates that if appropriate parameters are selected in consideration of a double skewed rotor, the tooth harmonic can be greatly reduced and the electromagnetic excitation force can be also reduced, thus the machine can obtain a better level of noise and vibration. In this paper, most of the parameters in the

different parts are the same including the same core length $l$, the same skew width $b_{sk}$, but the each part is towards the opposite direction. The skew width $b_s$ is selected as a stator tooth pitch, and angle difference $\alpha$ is selected as a half of the rotor pitch. What's more, as the current in middle ring is just the half of the current in the rotor bar, the middle ring can be designed very thin. All these are the key to design a double skewed rotor.

## 3. Analysis of Multi-slice Model

The normal skewed slot rotor can be simulated with 2D model in many finite element analysis softwares in general. However, due to the special structure of the double skewed slot rotor, the simulation is often carried out with 3D model. And it will cost a lot of computer memory storage and the simulation will also take much time. Thus, a multi-slice model is proposed in this paper on account of the double skewed slot rotor. Fig. 4 shows the equivalent circuits of a double skewed rotor. The induced electromotive force caused by all kinds of air-gap flux density can be transformed into an equivalent voltage source in each part including $V_{b1}$ and $V_{b2}$. $R_e$, $R_b$ and $R_m$ are the equivalent resistances of the end ring, rotor bar and the middle ring respectively. $I_{b1}$ and $I_{b2}$ are the equivalent currents of the rotor bar in each part respectively.

Take the stator tooth harmonic into consideration the equivalent voltages can be expressed as

$$\begin{cases} V_{b1}(\theta,t,z) = E_{b1}\cos(\nu\theta - \omega_1 t - \varphi_\nu - \nu\dfrac{b_{sk}z}{Rl}) \\ V_{b2}(\theta,t,z) = E_{b2}\cos(\nu\theta - \omega_\nu t - \varphi_\nu - \nu\dfrac{b_{sk}z}{Rl} - \nu\alpha) \end{cases} \tag{23}$$

As all the induced electromotive force is caused by the power supply on the stator side, the equivalent voltages can be transformed into the stator side. The equivalent voltage sources at different parts can be expressed as

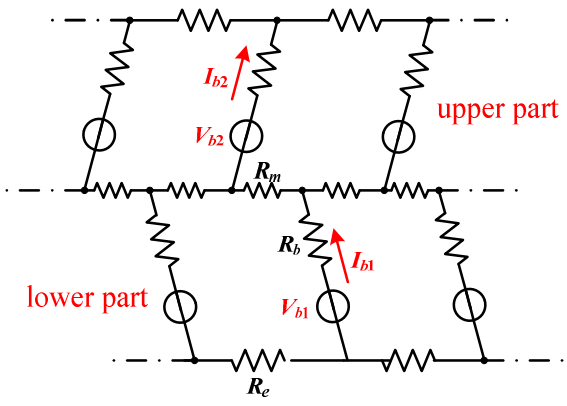


**Fig. 4.** Equivalent circuit of a double skewed rotor

$$\begin{cases} V_{s1}(\theta,t,z) = E_{s1}\cos(\theta - \omega_1 t - \varphi_0 - \dfrac{b_{sk}z}{Rl}) \\ V_{s2}(\theta,t,z) = E_{s2}\cos(\theta - \omega_1 t - \varphi_0 - \dfrac{b_{sk}z}{Rl} - \alpha) \end{cases} \tag{24}$$

The main idea of the multi-slice model is to divide the skewed slot rotor into several straight slot rotors which is numbered from 1 to M in Fig. 5. And there is a mechanical angle $\Delta\theta_m$ difference between different slices.

The equivalent circuit of multi-slice model of a double skewed rotor is shown in Fig. 6. It can be seen that when the skewed slot of each slice is replaced by an equivalent straight slot, the induced electromotive force of Slice $m$ will be also transformed into the following forms

$$\begin{cases} V_{b1-m}(\theta,t,z) = E_{b1}\cos(\nu\theta - \omega_1 t - \varphi_\nu - \nu\dfrac{b_{sk}z}{Rl}\cdot\dfrac{m}{M}) \\ V_{b2-m}(\theta,t,z) = E_{b2}\cos(\nu\theta - \omega_1 t - \varphi_\nu - \nu\dfrac{b_{sk}z}{Rl}\cdot\dfrac{m}{M} - \nu\alpha) \end{cases} \tag{25}$$

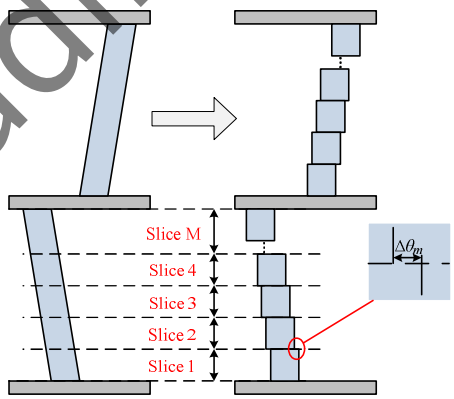


**Fig. 5.** Multi-slice model of a double skewed rotor

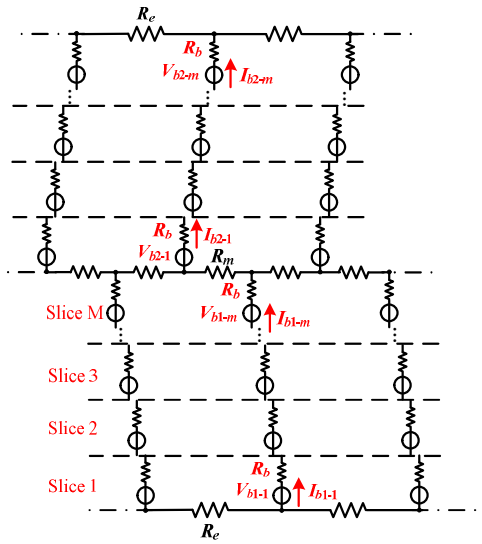


**Fig. 6.** Equivalent circuit of multi-slice model of a double skewed rotor

And the equivalent voltage sources in each slice in stator side can be expressed as

$$\begin{cases} V_{s1-m}(\theta,t,z) = E_{s1}\cos(\theta-\omega_1 t-\varphi_0-\dfrac{b_{sk}z}{Rl}\cdot\dfrac{m}{M}) \\ V_{s2-m}(\theta,t,z) = E_{s2}\cos(\theta-\omega_1 t-\varphi_0-\dfrac{b_{sk}z}{Rl}\cdot\dfrac{m}{M}-\alpha) \end{cases} \quad (26)$$

## 4. Simulation and Calculation

In this study, a four-pole 380V 7.5kW three-phase squirrel cage induction motor is simulated with the software of Maxwell Ansoft. The number of slots of the stator and rotor are 48 and 44, respectively. The finite element model of the double rotor motor is shown in Fig. 7. As shown in Fig. 7(a), the machine is divided into several slices along the axial direction in each part. The equivalent 2D model of each slice is shown in Fig. 7(b). As shown in Fig. 7(b), the rotor turns around $O$ with an angle of $\Delta\theta m$. It represents the difference in the mechanical angle as shown in Fig. 5 and Fig. 7.

Obviously, a larger number of slices may improve the simulation result, but this would be computationally less efficient. Thus, the rotor is divided into seven slices in each part in this work to guarantee accuracy and a fast simulation. The multi-slice model shown in Fig. 5 and Fig. 7 can be realised by requiring each slice of the rotor to move by the mechanical angle along the axial direction. The mechanical angle difference of Slice $m$ can be expressed as

$$\Delta\theta_m = \frac{7.5°}{6}m = 1.25°m \qquad m\in[0,6] \quad (27)$$

where 7.5° is the angle of the skewed slot. Furthermore, the excitations on the stator side at different positions along the axial direction in a skewed slot machine are different. Therefore, the stator excitations need to be changed in each slice. Taking phase A in Slice $m$ in Fig. 7(b) into consideration, according to (25) and (26), the voltage excitation on the stator side can be expressed in the following forms

$$v_m = 220\sqrt{2}\cos(100\pi t-\frac{2p\pi}{Z_1}\cdot\frac{m}{6}) \qquad m\in[0,6]. \quad (28)$$

Eqs. (27) and (28) show how the rotor mechanical angle

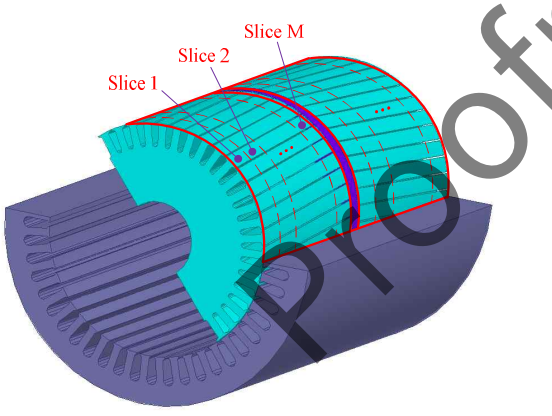


(a)

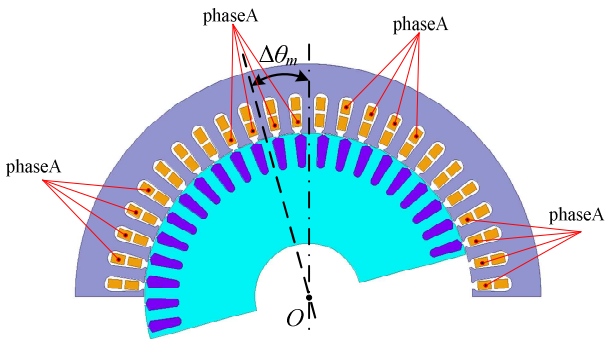


(b)

**Fig. 7.** Finite element model: (a) 3D finite element model. (b) Equivalent 2D finite element model

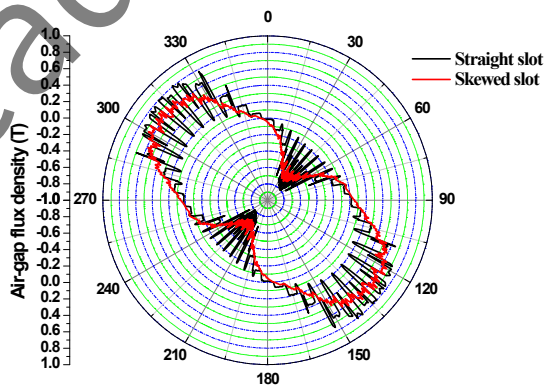


**Fig. 8.** Air-gap flux density distributions of straight slot and skewed slot in rated-load condition

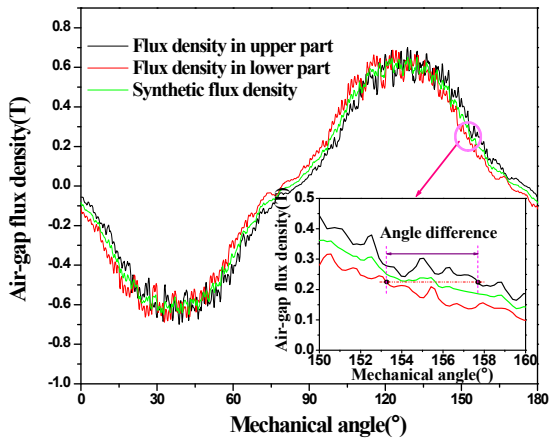


**Fig. 9.** Air-gap flux density distributions of different parts in rated-load condition

difference and the voltage excitation are set in each slice in the finite element simulation according to the analysis in section 3.

Fig. 8 shows the air-gap flux density distributions of straight and normal skewed slots in the rated-load condition. The curve is much smoother for the skewed slot condition than for the straight slot. Fig. 9 exhibits the air-gap flux density distributions in the two parts shown in Fig. 2 and Fig. 4. The flux density is obtained by calculating the average of the flux density in different slices exactly. It can be seen that both of the two curves are very smooth and that they approximate the shape of a sine wave. There is also an angle difference between the two curves. The angle difference in Fig. 9 is found to be approximately 4° in mechanical degrees and it can be transformed into $\pi/22$ in electrical degrees, thereby corresponding to the analysis in (26).

Fig. 10 shows the details of the 1st stator tooth harmonic, namely the 23rd and 25th harmonics of different parts and the synthetic flux density in the double skewed rotor. It is very clear that the amplitudes of the tooth harmonics in the two different parts are almost the same because the structure of each part is the same; however, the two curves have opposite phases. The phase difference transformed into electrical degrees is approximately π, which also corresponds to the analysis in (26). This indicates that a further reduction in the 23rd harmonic of the synthetic flux density would be possible. In addition, the distribution of the other 1st stator tooth harmonic is almost the same. Furthermore, the phase difference of the 25th harmonic is also approximately π; however, the angle difference is smaller than that of the 23rd because the angle of the skewed slot in the 23rd is closer than that of the 25th.

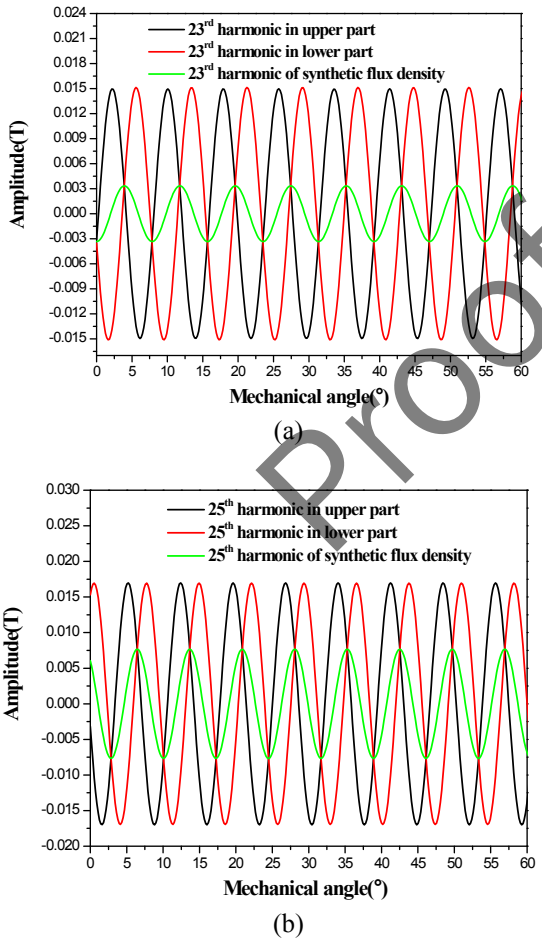


**Fig. 10.** Comparison of the 23rd and 25th harmonics of air-gap flux density in rated-load condition in double skewed rotor machine: (a) 23rd harmonics of air-gap flux density. (b) 25th harmonics of air-gap flux density

Fig. 11 and Table 1 provide the exact simulation results of the air-gap flux density obtained for the straight and skewed rotors. It can be seen that the fundamental harmonics of the straight slot and the skewed slot rotor are almost the same, and that those of the straight slot are a little larger than those of the skewed slot. This can be explained by considering that the skewed technology is also likely to affect the fundamental, thereby causing the amplitude to be reduced slightly. This corresponds to the traditional theory and the "skewed factor" is often selected to account for the influence [23]. Taking the 1st stator tooth harmonic into consideration, it is obvious that the 23rd and 25th harmonics are almost 0.12 T and 0.09 T, respectively, for the straight slot rotor. However, the harmonics in both parts of the skewed rotor are around 0.015 T. Furthermore, the synthetic harmonics were reduced the most, and the 23rd and 25th harmonics are 0.0033 T and 0.0077 T, respectively. All these results are a consequence of the influence of the phase shift of the middle ring.

**Table 1.** Harmonics of air-gap flux density

| Order | Straight slot (T) | Lower part (T) | Upper part (T) | Synthetic (T) |
|---|---|---|---|---|
| | 0.5783 | 0.5754 | 0.5750 | 0.5735 |
| 23 | 0.1208 | 0.0150 | 0.0151 | 0.0033 |
| 25 | 0.0930 | 0.0170 | 0.0169 | 0.0077 |

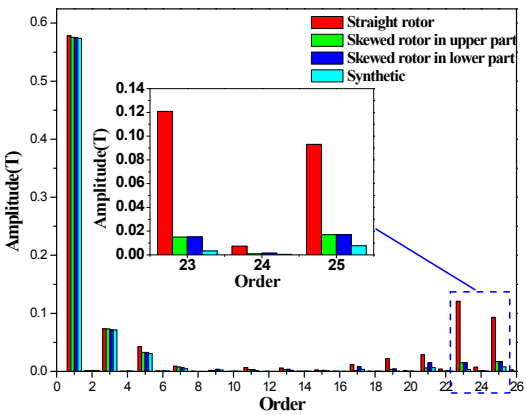


**Fig. 11.** Comparison of the harmonics of the straight slot and skewed slot rotors under rated-load condition

**Table 2.** Harmonics of electromagnetic excitation forces

| Order | Straight slot (Pa) | Lower part (Pa) | Upper part (Pa) | Synthetic (Pa) |
|---|---|---|---|---|
| 0 | 154610 | 135200 | 134989 | 135095 |
| 1 | 92673 | 82151 | 81832 | 81173 |
| 2 | 8202 | 9008 | 8766 | 8661 |
| 3 | 12809 | 8141 | 7856 | 7008 |
| 4 | 3184 | 2287 | 1681 | 1293 |

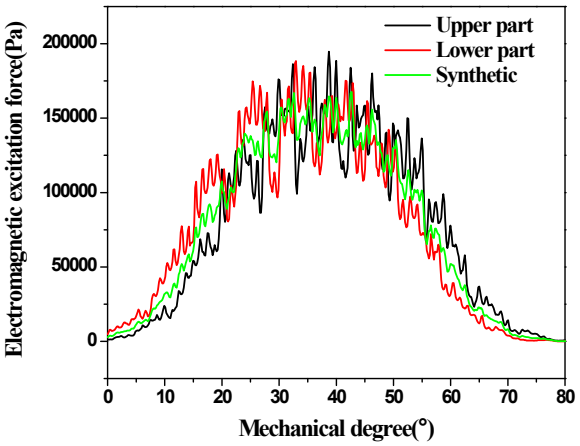


**Fig. 12.** Electromagnetic excitation forces: distributions of different parts of the double skewed rotor under no-load conditions.

According to the Maxwell stress tensor method expressed in (16), the distributions of the electromagnetic excitation force can easily be obtained. Fig. 12 shows the electromagnetic excitation force distributions. The curves are very similar to the air-gap flux density distributions. Similarly, there is an angle difference between the two curves. The conventional theory reveals that the noise and vibration of the motor is mainly affected by the electromagnetic excitation force of which the order is less than 4. Table 2 lists the main electromagnetic excitation forces related to the noise and vibration with the order ranging from 0 to 4. Moreover, the simulation results in Table 2 indicate that the force of the 1st and 3rd order can be reduced as well. They are reduced even more when the structure is changed to that of a double skewed rotor. However, the fundamental harmonics of the electromagnetic excitation force are almost the same in the two parts and the 2nd order harmonic increases a little in both the normal skewed rotor and double skewed rotor machines. This verifies the correctness of the theory.

## 5. Conclusion

This paper presents a mechanism according to which a skewed slot can reduce the tooth harmonic. We reduced the electromagnetic excitation force by introducing a special structure in the form of a double skewed slot rotor and present the main design theory of the double skewed slot machine in this paper. The results presented here enabled us to conclude that the skew width for each skewed slot is a stator tooth pitch and the angle difference between the two skewed slots is a half rotor tooth pitch in general.

Because the use of a 3D model is computationally intensive, a special simplified 2D model of the double skewed slot rotor with a multi-slice method is proposed. Finite element analysis was used to obtain the distributions of the air-gap flux density and the electromagnetic excitation force under different conditions. From this we concluded that the skewed slot has a great effect on reducing the stator tooth harmonics of both the air-gap flux density and the electromagnetic excitation force. On account of the angle difference between the two skewed slots, the distributions of the 1st order stator harmonic, i.e. the 23rd and 25th harmonics, have a phase difference of $\pi$. Thus, the synthetic harmonics of the air-gap flux density and the electromagnetic excitation force were found to be very small. This verifies the correctness of the theory and lays the foundation for the investigation of double skewed rotor motors.



## Acknowledgements

This work was supported by the National Natural Science Funds of China (No.51677051 and No.51377039), and Anhui Province Key Laboratory of Large-Scale Submersible Electric Pump and Accoutrements.

## References

[1] S. B. Yu, and R. Y. Tang. "Electromagnetic and mechanical characterizations of noise and vibration in permanent magnet synchronous machines," *IEEE Trans. Magn.*, vol. 42, no. 4, pp. 1335-1338, Apr. 2006.

[2] D. H. Cho, and K. J. Kim. "Modelling of electromagnetic excitation forces of small induction motor for vibration and noise analysis," *IEE Proceedings-Electric Power Applications*, vol. 145, no. 3, pp. 199-205, May. 1998

[3] C. L. Xia, Z. Zhang, and Q. Geng. "Analytical Modeling and Analysis of Surface Mounted Permanent Magnet Machines With Skewed Slots," *IEEE Trans. Magn.*, vol. 51, no. 5, Article#:8104508, May. 2015.

[4] H. Karmaker, and A. M. Knight. "Investigation and Simulation of Fields in Large Salient-Pole Synchronous Machines With Skewed Stator Slots," *IEEE Trans. Energy Convers.*, vol. 20, no. 3, pp. 604-610, Sept. 2005.

[5] I. Hirotsuka, Y. Tsubouchi, and K. Tsuboi. "Effects of slot combination and skew slot on the electromagnetic

vibration of a 4 pole capacitor motor under load condition," *Electrical Machines and Systems, 2005. ICEMS 2005. Proceedings of the Eighth International Conference on. IEEE*., Nanjing, China, Sept. 2005.
[6] D. H. Im, J. H. Chang, S. C. Park, and et al. "Analysis of radial force as a source of vibration in an induction motor with skewed slots," *IEEE Trans. Magn.*, vol. 33, no. 2, pp. 1650-1653, Mar. 1997.
[7] H. Kometani, Sakabe, Shigekazu, and et al. "3-D analysis of induction motor with skewed slots using regular coupling mesh," *IEEE Trans. Magn*., vol. 36, no. 4, pp. 1769-1773, Jul. 2000.
[8] K. Yamada, Y. Takahashi, and K. Fujiwara. "Simplified 3D Modeling for Skewed Rotor Slots with End-ring of Cage Induction Motors," *IEEE Trans. Magn*., vol. 52, no. 3, Article#:8101604, Mar. 2016.
[9] K. Yamazaki. "A quasi 3D formulation for analyzing characteristics of induction motors with skewed slots," *IEEE Trans. Magn*., vol. 34, no. 5, pp. 3624-3627, Sept. 1998.
[10] Y. Kawase, T. Yamaguchi, Z. P. Tu, and et al. "Effects of Skew Angle of Rotor in Squirrel-Cage Induction Motor on Torque and Loss Characteristics," *IEEE Trans. Magn*., vol. 45, no. 3, pp. 1700-1703, Mar. 2009.
[11] G. D. Kalokiris, T. D. Kefalas, A. G. Kladas, and et al. "Special air-gap element for 2-D FEM analysis of electrical Machines accounting for rotor skew," *IEEE Trans. Magn*., vol. 41, no. 5, pp. 2020-2023, May. 2005.
[12] J.J.C. Gyselinck, L. Vandevelde, J.A.A. Melkebeek. "Multi-slice FE modeling of electrical machines with skewed slots-the skew discretization error," *IEEE Trans. Magn*., vol. 37, no. 5, pp. 3233-3237, Sept. 2001.
[13] S. L. Ho, W. N. Fu, and H. C. Wong. "Direct modeling of the starting process of skewed rotor induction motors using a multi-slice technique," *IEEE Trans. Energy Convers*., vol. 14, no. 4, pp. 1253-1258, Dec. 1999.
[14] G. H. Muller, and C. F. Landy. "A novel method to detect broken rotor bars in squirrel cage induction motors when interbar currents are present," *IEEE Trans. Energy Convers*., vol. 18, no. 1, pp. 71-79, Mar. 2003.
[15] A. Lamine, and E. Levi. "Dynamic induction machine modelling considering the stray load losses," *Universities Power Engineering Conference, 2004. UPEC 2004. 39th International. IEEE*, Bristol, UK, Sept. 2004.
[16] L. Wang, X. H. Bao, C. Di, and et al. "Effects of Novel Skewed Rotor in Squirrel-Cage Induction Motor on Electromagnetic Force," *IEEE Trans. Magn*., vol. 51, no. 11, Article#:8114204, Nov. 2015.
[17] W. Fei, and Z. Q. Zhu. "Comparison of cogging torque reduction in permanent magnet brushless machines by conventional and herringbone skewing techniques," *IEEE Trans. Energy Convers*., vol. 28, no. 3, pp. 664-674, Sept. 2013.
[18] H. Ahn, G. Jang, J. Chang, and et al. "Reduction of the torque ripple and magnetic force of a rotatory two-phase transverse flux machine using herringbone teeth," *IEEE Trans. Magn*., vol. 44, no. 11, pp. 4066-4069, Nov. 2008.
[19] T. J. Wang, F. Fang, X. S. Wu, and et al. "Novel Filter for Stator Harmonic Currents Reduction in Six-Step Converter Fed Multiphase Induction Motor Drives," *IEEE Trans. Power Electron*., vol. 28, no. 1, pp. 498-506, Jan. 2013.
[20] D. G. Dorrell. "Calculation of unbalanced magnetic pull in small cage induction motors with skewed rotors and dynamic rotor eccentricity," *IEEE Trans. Energy Convers*., vol. 11, no. 3, pp. 483-488, Sept. 1996.
[21] W. Bernhard, O. Biro, S. Rainer, and et al. "Computation of rotating force waves in skewed induction machines using multi-slice models," *IEEE Trans. Magn*., vol. 47, no. 5, pp. 1046-1049, May. 2011.
[22] Ho, S. L., W. N. Fu, and H. C. Wong. "Estimation of stray losses of skewed rotor induction motors using coupled 2-D and 3-D time stepping finite element methods," vol. 34, no. 5, pp. 3102-3105, Sept. 1998.
[23] J. Pyrhonen, T. Jokinen, and V. Hrabovcova. *Design of rotating electrical mechines*. John Wiley& Sons, Ltd, 2008, pp. 250-251.



**Xiaohua Bao** He received the B.S. degree in 1996, the M.Sc. degree in 2002 and the Ph.D. degree in 2008, all in electrical engineering from Hefei University of Technology, Hefei, China. He joined the School of Electrical Engineering and Automation, Hefei University of Technology and was promoted to Professor, in 2012. He was a visiting Scholar with Virginia Polytechnic Institute and State University, U.S. His main research interests are in the field of motor design, magnetic field analysis, and finite element analysis.

**Chong Di** He received the B.S. degree in 2014 and the M.Sc. degree in 2017, both in electrical engineering from Hefei University of Technology, Hefei, China. He is currently working toward the Ph.D degree in electrical engineering at Lappeenranta University of Technology, Finland. His main research interests are in the field of motor design, finite element analysis and electromagnetic field analysis.

**Yang Zhou** He received the B.S. degree in 2014 in electrical engineering from Hefei University of Technology, Hefei, China. He joined the School of Electrical Engineering and Automation, Hefei University of Technology as a doctoral student from 2014. His main research interests are in the field of rotor eccentricity, finite element analysis and electro-magnetic field analysis.